J Therm Spray Tech (2017) 26:1898–1907
https://doi.org/10.1007/s11666-017-0640-8

PEER REVIEWED

Effect of Heat Treatment on Microstructure and Mechanical Properties of A380 Aluminum Alloy Deposited by Cold Spray

Xiang Qiu[1,2] · Ji-qiang Wang[1] · Naeem ul Haq Tariq[1,3,4] · Lawrence Gyansah[1,3] · Jing-xuan Zhang[5] · Tian-ying Xiong[1]

Submitted: 13 July 2017 / in revised form: 30 August 2017 / Published online: 13 September 2017

Abstract The microstructure and mechanical properties of cold-sprayed bulk A380 alloy were investigated after heat treatment at various conditions, using optical and electron microscopy and tensile and hardness tests, respectively. The results revealed that heat treatment increased the strength and ductility of the cold-sprayed A380 alloy deposits compared with as-sprayed state. Heat treatment showed two different effects on the mechanical properties of the deposits. On the one hand, it resulted in effective diffusion at interparticle boundaries that altered the particle bonding mechanism from pure mechanical interlocking to metallurgical bonding. Thus, the strength and ductility of the material were greatly enhanced. On the other hand, interparticle diffusion during high-temperature heat treatment resulted in growth of the Si phase and pores, which ultimately reduced the strength and elongation of the alloy. This observation was consistent with the hardness results, which showed a decreasing trend with increase of the heat treatment temperature.

Keywords cold spray · heat treatment · mechanical properties · microstructure

✉ Ji-qiang Wang
jqwang11s@imr.ac.cn

✉ Tian-ying Xiong
tyxiong@imr.ac.cn

[1] Institute of Metal Research, Chinese Academy of Sciences, Shenyang 110016, People's Republic of China

[2] School of Materials Science and Engineering, University of Science and Technology of China, Shenyang 110016, People's Republic of China

[3] University of Chinese Academy of Science, No. 19 (A) Yuquan Road, Shijingshan District, Beijing 100049, People's Republic of China

[4] Department of Metallurgy and Materials Engineering, Pakistan Institute of Engineering and Applied Science, Nilore, Islamabad, Pakistan

[5] Qiushi Honors College, Tianjin University, Tianjin 300350, People's Republic of China

Introduction

Cold spray is a robust coating technology based on the principle of gas dynamics. It was discovered in 1990 (Ref 1). When their velocity exceeds a critical value (Ref 2, 3), particles are deposited on the substrate surface after severe plastic deformation due to the collision. The main effect in the bonding mechanism is shear instability caused by thermal softening and adiabatic heating, resulting in high-strain-rate deformation of the feedstock (Ref 2, 4). The temperature in the cold-spray process remains well below the melting point of the sprayed material, enabling production of dense coatings with less oxidation and no phase transformation. This technique has been extensively used to produce a wide range of coatings such as metallic, composite, nanocrystalline, and amorphous materials (Ref 5-11). Another interesting characteristic of the cold-spray process is the relatively low residual stress in the deposited material, which makes it suitable for additive manufacturing of high-technology engineering products (Ref 12-14).

As a developing technology, cold-spray additive manufacturing is still in its infancy. Currently, there is a lack of selection criteria, including for the spray process, deposition material, and organizational structure, as well as other basic research work. Recently, some researchers have carried out preliminary studies on additive manufacturing via production of thick metal deposits using the cold-spray

process and studied the resulting mechanical properties including hardness and tensile properties. Huang et al. (Ref 15) studied the mechanical properties of Al, Cu, Ti, and 316L stainless-steel coatings after application of heat treatment at different conditions. They reported that the heat treatment process could significantly alter the mechanical properties of the as-sprayed deposits. For dense coatings such as Cu, the best mechanical properties could be obtained by recrystallization during heat treatment near the recrystallization temperature. However, the tensile strength of porous coatings such as cold-sprayed Al and stainless steel 316L was lower than those of the bulk materials, since heat treatment could only heal a few defects in the coating. Eason et al. (Ref 16) successfully deposited more than 25-mm-thick pure copper on a vacuum hot-pressed copper substrate using cold spray technology. That study revealed that the microhardness of the annealed deposit was lower than that of the as-sprayed deposit but higher than that of a bulk Cu substrate fabricated by powder metallurgy. This behavior occurred due to localized grain refinement facilitated by the high degree of cold work during the cold-spray process. These results clearly highlight the potential of the cold-spray technique for preparing strong bulk materials with performance and properties that might exceed those of their powder metallurgical counterparts. However, preparation of thick alloy deposits containing precipitation phases as well as their effects on mechanical properties are seldom reported. Rokni et al. (Ref 7) studied the relationship between the local microstructure and mechanical properties of cold-sprayed 7075 aluminum alloy with thickness of 8.5 mm. They found that particle–particle interface regions had higher nanohardness, smaller grain size, and lower dislocation density compared with the particle interiors. This mainly occurs due to formation of ultrafine grain (UFGs) during the dynamic recrystallization phenomenon. Similar conclusions were reached for the cold-sprayed 6061 aluminum alloy deposit.

Al-Si alloy is widely used in the automotive and aerospace industries due to its light weight, high strength, as well as excellent wear resistance (Ref 17-20). The mechanical properties of Al-Si alloys can be improved by heat treatment at suitable conditions (Ref 21). A380 alloy is most commonly applied for cylinder heads and engine blocks. In the past, researchers have performed a lot of work that has mainly concentrated on the casting process and control of the microstructure (Ref 22-26). However, the cold-spray technique is rarely utilized for preparing A380 alloy coatings or bulk deposits. Moreover, the microstructure and mechanical properties of cold-spray A380 alloy deposits have not been investigated to date.

In this work, an 8-mm-thick deposit of A380 alloy was successfully fabricated by the cold-spray process. The microstructure and mechanical properties of the as-sprayed material as well as after heat treatment at different conditions were investigated in detail.

Experimental Procedures

Raw Material

The powder used in this experiment was commercially available gas-atomized A380 alloy powder (Al-8.74Si-3.30Cu-0.35Zn-0.27Fe-0.24Mn). A laser particle size analyzer (Mastersizer 2000, Malvern, UK) was used to probe the particle size distribution. A cylindrical carbon-steel rod with diameter of 25 mm was used as substrate. Prior to deposition, the substrate was cleaned with acetone in an ultrasonic bath cleaner then sandblasted using Al_2O_3 grit to remove the oxide layer.

Cold-Spray Process

A home-made cold-spray device equipped with a convergent–divergent (de Laval) cylindrical polymer nozzle was used for alloy deposition. The distance from throat (diameter 2.5 mm) to exit (diameter 7.1 mm) of the nozzle was 58.5 mm. Compressed air was used as carrier gas and accelerating gas. During the cold-spray process, the temperature was maintained at 400 °C and the gas pressure was kept at 2.6 MPa. Steel substrate with diameter of 35 mm was held in a chuck rotating at speed of 5 rpm. The spray gun was moved at linear speed of 0.02 mm/s above the substrate at standoff distance of 10 mm. The powder feed rate was fixed at 20 g/min. An 8-mm-thick coating was deposited.

Heat Treatment

To improve the strength and ductility, heat treatment was carried out at various temperatures ranging from 200 to 500 °C. Specimens were annealed in argon atmosphere for 2, 4, 6, 8, 10, 12, 14, 16, 18, and 24 h. Hardness measurements were carried out for all specimens while a specimen heat treated for 10 h was selected to study the tensile behavior of the deposited alloy.

Microstructure Evaluation

The surface morphology and cross-sectional microstructure of the alloy powders were characterized by scanning electron microscopy (SEM). SEM was also used to observe the fracture surface of tensile test samples, while optical microscopy (OM) was employed to examine the cross-section of the alloy deposit after heat treatment at different

conditions. Before observing the cross-section of the deposits under OM, the specimens were cold-mounted in denture acrylic, then ground, and polished using standard metallographic preparation procedures. Etching solution containing 0.5 mL HF and 100 mL purified water was used to etch the specimens. X-ray diffraction (XRD) analysis of the powder and deposits was performed using a Philips X'Pert MPD diffractometer (Cu K_α radiation, 0.02°/s scan rate). The porosity of the specimens was calculated using metallographic image analysis software. To verify the accuracy of the porosity values, the density of the specimens was also measured using a density meter (XS105 Dual Range, Mettler Toledo, Switzerland).

Mechanical Properties

Microhardness

Microhardness measurements were performed on the cross-section of the deposits after heat treatment at different conditions using a Vickers microhardness tester (AMH43, Leco, USA) under 200 g load with 15 s holding time. For each sample, at least seven indentations were taken at random locations, and the average value as well as the standard deviation calculated.

Tensile Tests

Tensile tests were performed on an electronic dynamic and static universal testing machine (E1000, Instron, UK). A total of 18 samples were tested, including 3 samples for each condition: as-cast, as-sprayed, and heat-treated (at 200, 300, 400, or 500 °C for 10 h). Figure 1 shows the dimension of the tensile test samples. After heat treatment, the deposit was cut from the substrate bars and machined into a tensile specimen by using an electric discharge machine. Finally, tensile test specimens were ground with SiC sandpapers from 400# to 3000# to reduce surface defects/scratches before performing the test.

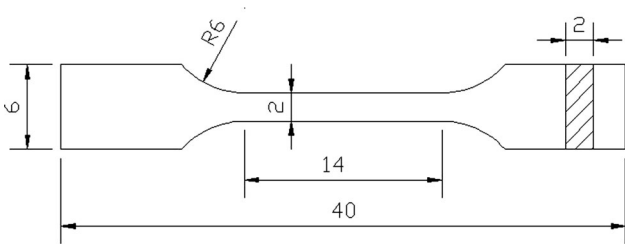

Fig. 1 Dimensions of tensile test samples

Results and Discussion

Powder Characterization

The particle size distribution of the A380 powder (Fig. 2) exhibited $d(0.1)$, $d(0.5)$, and $d(0.9)$ values of 27.3, 39.5, and 56.9 μm, respectively. Figure 3(a) shows the morphology of the A380 gas-atomized powder, exhibiting near-spherical shape. Figure 3(b) shows the rapidly quenched gas-atomized cross-section microstructure of the particles. Fine-scaled dendritic microstructure can be clearly observed, with Si phase formed between primary α-Al dendrite arms. Primary silicon even formed in the hypoeutectic Al-Si alloy due to the high cooling rates. In Fig. 2(b), the bright phase with rod-like morphology was revealed to be a Cu-rich phase by energy-dispersive x-ray spectroscopy (EDS), subsequently identified as Al_2Cu (θ phase) by XRD analysis. This phase is considered to act as a strengthening phase for the deposited alloy (Ref 27). α-Al and Si peaks were also identified in the XRD pattern of the starting powder, as is evident from Fig. 4(a).

Microstructure Analysis

XRD Results

Figure 4 shows the x-ray diffraction (XRD) patterns of A380 alloy powder and cold-sprayed deposits after heat treatment at different conditions. The Si, α-Al, and θ phase can be accurately identified. Moreover, the diffraction patterns of the deposits subject to heat treatment at different conditions were consistent with that of the initial powder, with no additional peaks being found. This indicates that no obvious phase transformation or oxidation

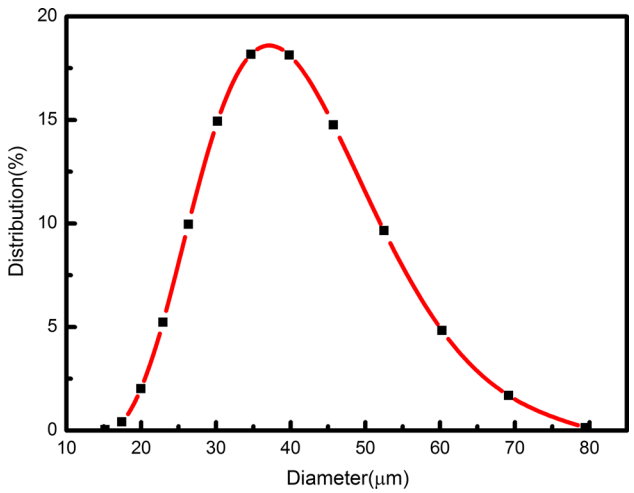

Fig. 2 Particle size distribution of A380 powder

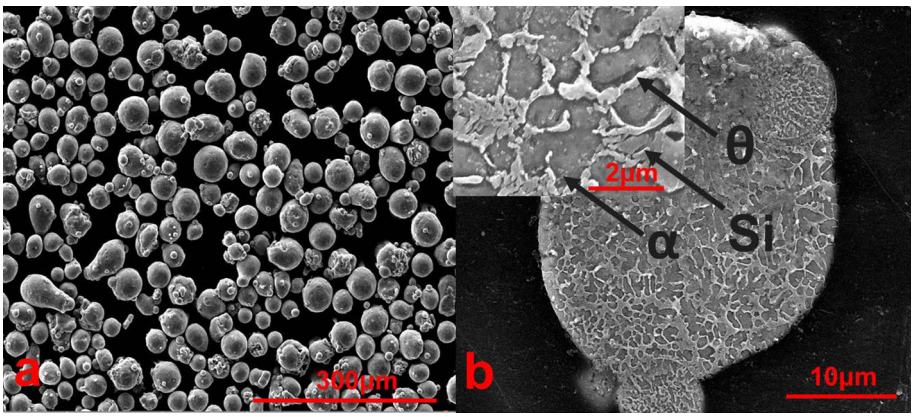

Fig. 3 Morphology (a) and cross-sectional microstructure (b) of A380 particles

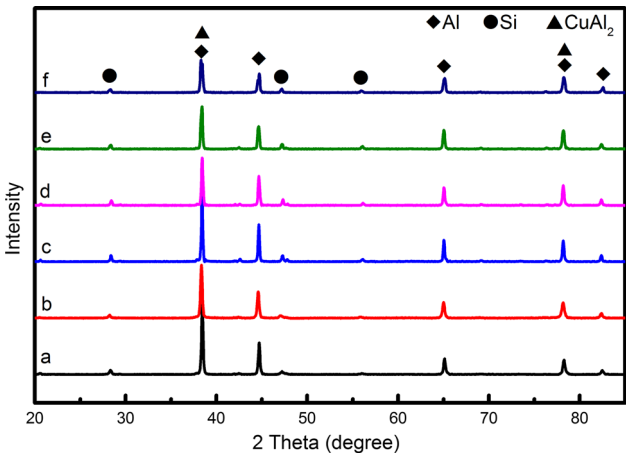

Fig. 4 XRD analysis for A380 powder (a), as-sprayed deposit (b), and after heat treatment at 200 °C (c), 300 °C (d), 400 °C (e), and 500 °C (f)

took place during the cold spray or heat treatment processes.

Microstructure Evolution

Figure 5(a), (b), (c), (d), and (e) show the etched cross-section microstructure of the deposits subject to heat treatment at different conditions. Note that eutectic Si appears black, whereas intermetallic (mainly Al_2Cu) appears light yellow after etching by aqueous HF solution. This observation is similar to typical optical micrographs of cast A380 alloys (Ref 27-29). During the cold-spray process, particles experience severe plastic deformation and form a relatively dense deposit. Nevertheless, some poorly bonded interparticle boundaries can be observed in Fig. 5(a). Furthermore, the Si phase showed a network distribution in the particles. In Fig. 5(b), the organizational structure is not significantly changed after heat treatment at 200 °C. Due to the effective diffusion, some of the boundaries between particles are difficult to distinguish. It can be observed in Fig. 5(c) that, on further increasing the heat treatment temperature to 300 °C, the composition of the coating homogenized and the dendritic branched characteristic disappeared, thereby forming small agglomerated dendrites. Figure 5(d) reveals that the Si phase was completely pelletized and tended to diffuse with a growing trend with further increase of the heat treatment temperature to 400 °C. Furthermore, some visible pores, approximately <2 μm in size, emerged. Further increase in the heat treatment temperature to 500 °C resulted in a more pronounced change in the organizational structure, as shown in Fig. 5(e). It can be clearly observed from this figure that Si phase mainly segregated at particle boundaries while its diameter sharply increased to 20 μm. Additionally, Al_2Cu phase was partially dissolved in the primary α-Al phase, consistent with the studies of Yang et al. (Ref 29) and Rosso et al. (Ref 30). Small pores disappeared at the expense of growth of large pores having size of about 10 μm (Fig. 5e).

It is worth mentioning that heat treatment at 200 °C did not result in any significant change in the microstructure of the deposit. This hints that the work-hardening effect, generated during the cold-spray process, is not removed by heat treatment at relatively low temperature. On increasing the temperature, the behavior of eutectic silicon phase in A380 aluminum alloy exhibited three stages: fragmentation, granulation, and coarsening. After heat treatment at the 300 °C condition, the thermal effect causes the eutectic silicon phase to become energetically unstable, resulting in its dissolution, diffusion, and breakage. Subsequently, under the combined effect of thermal action and irregular curvature, eutectic silicon starts to attain regular shape and forms granules to lower its surface energy. This process occurs mainly at the 400 °C heat treatment condition. Finally, the continuing granulation process results in coarse eutectic silicon phase driven by reduction of surface energy for the 500 °C heat treatment condition.

Figure 6(a) shows the porosity level of the deposits as determined by metallographic image analysis software. It can be observed that the porosity of the deposits was about

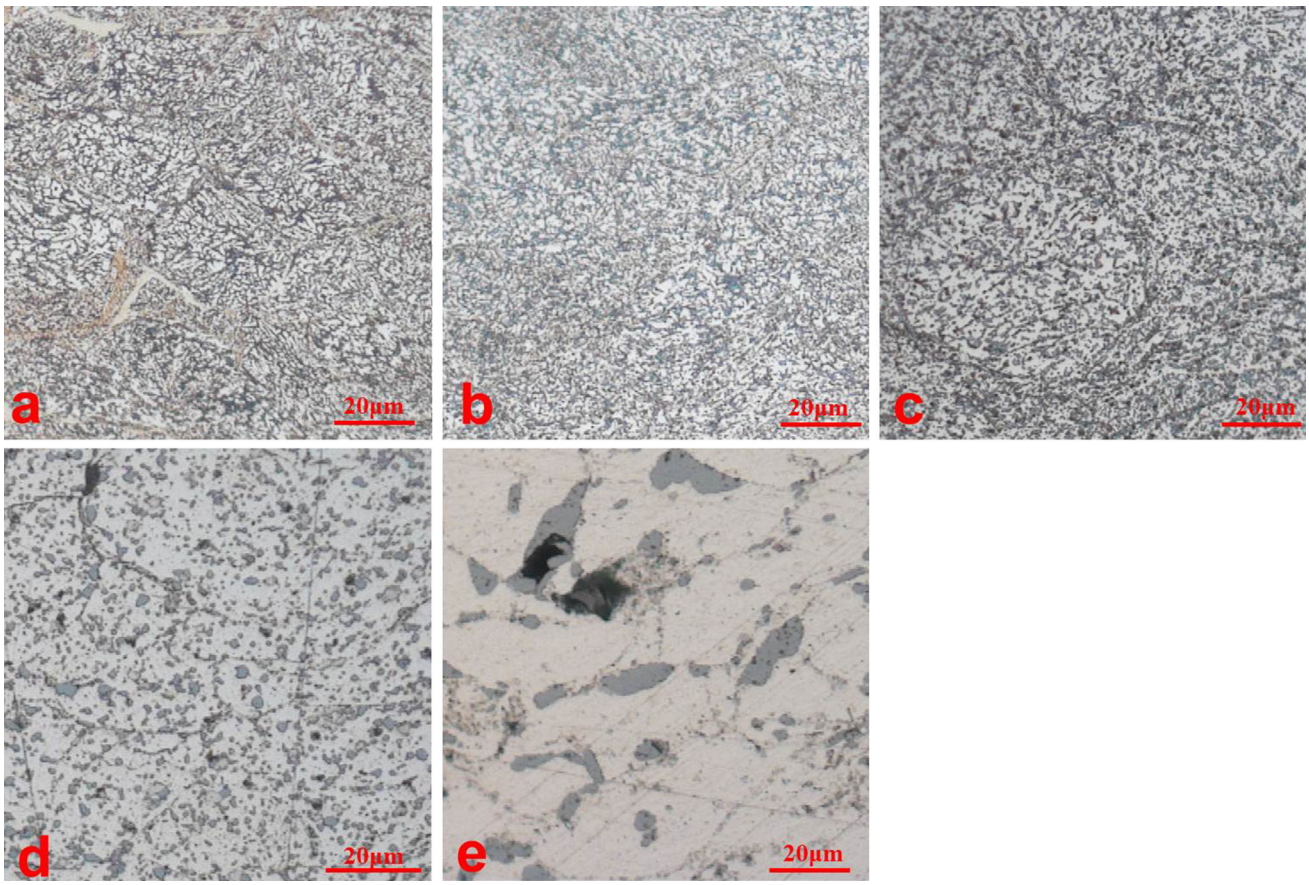

Fig. 5 Microstructure of A380 deposit: as-sprayed (a) and heat treated at 200 °C (b), 300 °C (c), 400 °C (d), and 500 °C (e)

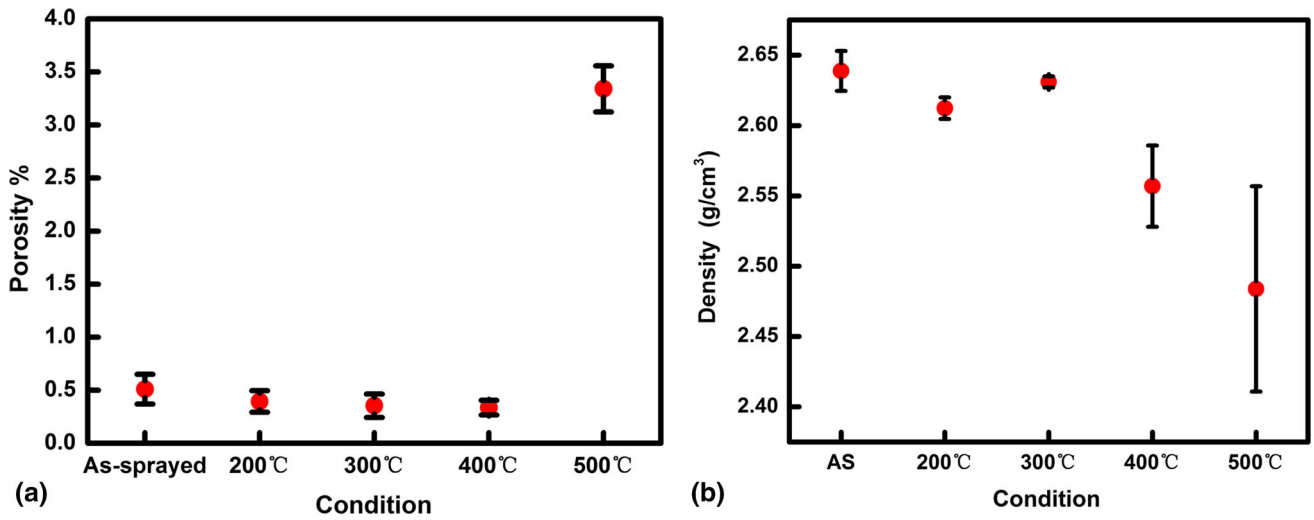

Fig. 6 Porosity (a) and density (b) of A380 deposits in as-sprayed and different heat-treated conditions

0.5 %. The porosity of the deposits reduced slightly after heat treatment at 200, 300, and 400 °C for 10 h. However, it is interesting to note that the porosity apparently increased up to about 3.5 % for the 500 °C heat treatment condition. Consistent with Fig. 5(d), a few large pores appeared for the 400 °C heat treatment condition. Figure 6(b) shows the results of density tests based on Archimedes principle. This corresponds with the porosity results for the density of the deposit, which were lower after heat treatment at 400 and 500 °C (less than 2.57 g/

cm^3) than for the other conditions (2.60-2.67 g/cm^3). This is probably due to reorganization and coalescence of small defects located at particle boundaries during the deformation process. Coddet et al. (Ref 31) and Al-Mangour et al. (Ref 32) also observed this phenomenon in 304 and 316L stainless-steel deposits, respectively. In Al-Mangour's opinion, the pores tend to be very small because of the severe work-hardening of the particles during the cold-spray process and develop from diffusion mechanisms occurring at high temperature.

Mechanical Properties

Microhardness

The microhardness of the deposits after annealing using different temperature and time conditions are presented in Fig. 7. Due to the high amount of work hardening during the cold-spray process, the as-sprayed deposits showed a higher microhardness level (131 ± 3.7 $HV_{0.2}$) than most of the heat-treated deposits. It can be observed that the microhardness decreased as the heat treatment temperature was increased for the same treatment duration. In general, it decreased with time at fixed heat treatment temperature. The value did not change significantly at the 200 °C heat treatment condition because this lower heat treatment temperature could not totally remove the work hardening generated during the cold-spray process. On further increase of the temperature to 300 °C, the microhardness profile displayed three stages: (1) a gradual decrease from 2 h to 10 h, (2) a steady stage with slightly fluctuation from 10 h to 16 h, and (3) a slower rate of decrease from 16 h to 24 h. This can be explained based on a recovery–recrystallization–grain growth theory (Ref 15). In stage 1, the work hardening as well as intensive plastic deformation generated in the cold-spray process were gradually removed over time. This is because the defect density as well as the internal stress were significantly reduced due to dislocation movement at high temperature. This recovery process leads to the decrease of the hardness and is finished after heat treatment for 10 h. At this time, diffusion at particle interfaces becomes more intensive and some strongly bonded particle interfaces are difficult to distinguish, as shown in Fig. 5. Recrystallization occurs in the deposits, generating fine grains that lead to increase in the hardness of the deposit. Further extension of the heat treatment time results in coarsening of fine grains and consequently a decrease in hardness. In stage 2, recrystallization and grain growth processes proceed constantly, causing the hardness to remain dynamically balanced. The decrease of hardness in stage 3 is mainly dominated by grain growth while recrystallization is exhausted. With further increase of the heat treatment temperature to 400 °C, the hardness values sharply decreased within 2 h and the recrystallization as well as grain-growth process took place earlier than at 300 °C, as shown in Fig. 8. The grains will not grow further once they reach a certain extent, thus the hardness remains basically unchanged. Later, due to fusion, granulation, and coarsening of Si phase, the hardness gradually reduced. The hardness values changed slightly from 2 to 24 h for the 500 °C heat treatment condition. This indicates that the Si phase coarsening process is completed in 2 h at high temperature and further extension of the heat treatment time has little or no effect on the hardness of the material.

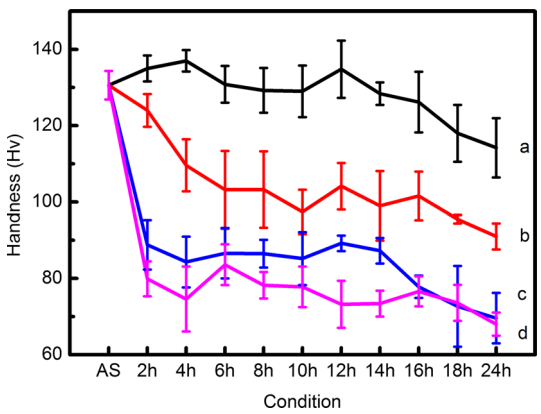

Fig. 7 Hardness as function of heat treatment temperature and time for cold-sprayed A380 deposit: heat treated at 200 °C (a), 300 °C (b), 400 °C, (c), and 500 °C (d)

Tensile Properties

Figure 8 shows representative stress–strain curves and the dependence of the ultimate tensile strength (UTS) and elongation (Elf) of cold-sprayed A380 deposits after heat treatment at different conditions. It can be observed from these curves that the work-hardening phenomenon occurs in the deposited A380 aluminum alloy. Both the tensile strength and elongation were very low for the as-sprayed deposit (114 ± 3 MPa UTS; 0.05 ± 0.03 % Elf), meaning that poorly combined particle boundaries dominate the strength of the material in spite of the work-hardening effect. An obvious effect on the strength is observed after heat treatment at 200 °C (182 ± 5 MPa UTS; 0.14 ± 0.02 % Elf) and 300 °C (186 ± 17 MPa UTS; 0.25 ± 0.04 % Elf). A significant increase in elongation was obtained after heat treatment at 400 °C (143 ± 8 MPa UTS; 0.93 ± 0.05 % Elf), while the UTS after heat treatment at 400 °C was decreased, potentially due to grain coarsening. On further increase of the heat treatment temperature to 500 °C, the tensile strength as well as elongation of the deposit decreased to 127 ± 10 MPa and 0.55 ± 0.14 %, respectively. For comparison with the

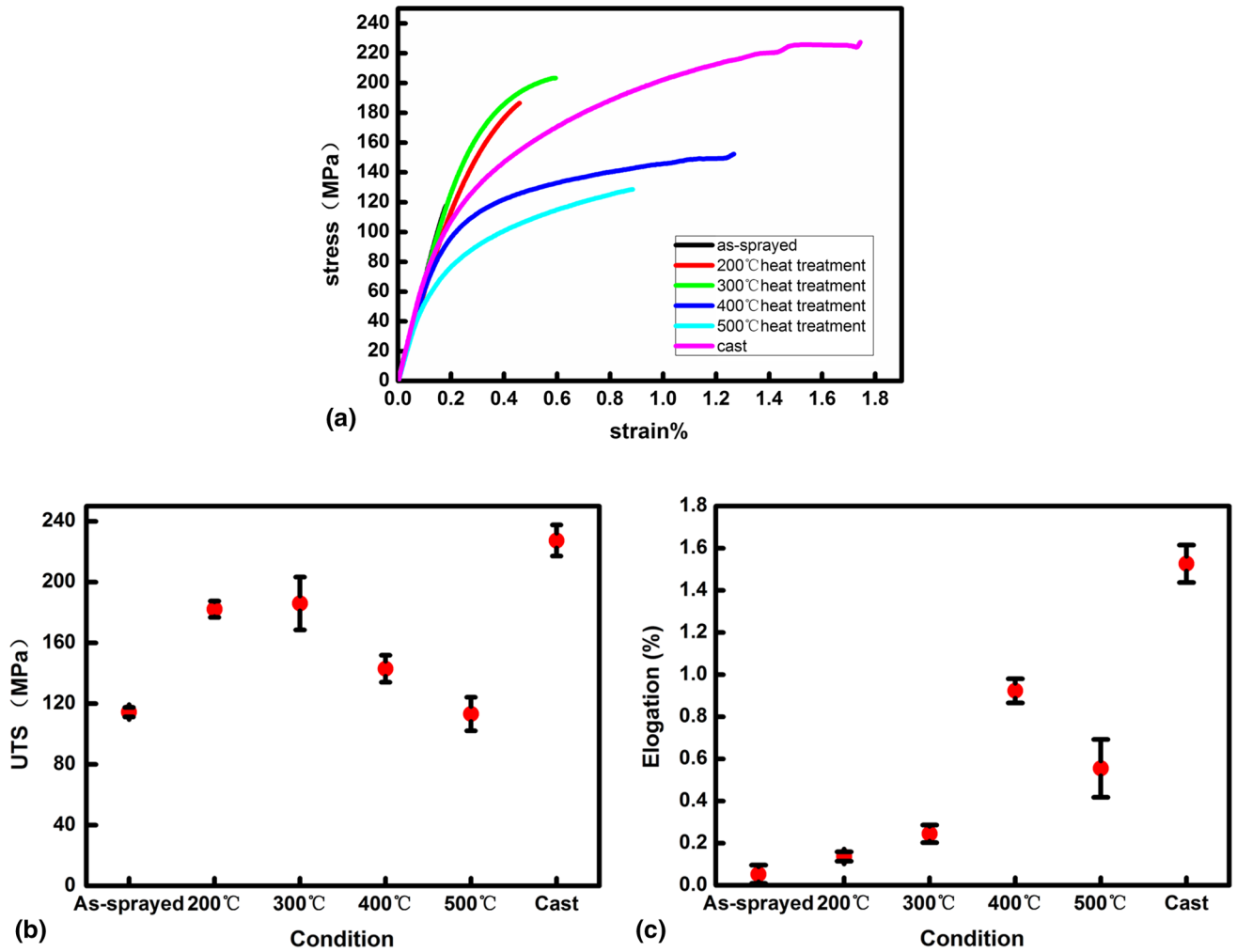

Fig. 8 Stress–strain curves (a), ultimate tensile strength (UTS) (b), and elongation (c) for tensile specimens of cold-sprayed A380 deposit under as-sprayed and different heat treatment conditions. The stress–strain curve of cast A380 alloy is also shown

cold-sprayed deposit, the tensile properties of as-cast samples (227 ± 10 MPa UTS; 1.52 ± 0.08 % Elf) are also shown in Fig. 8. The tensile strength of the sprayed samples after heat treatment at 300 °C was close to that of the as-cast samples, while the elongation of the sprayed samples after heat treatment at 400 °C was close to that of the as-cast samples.

Figure 9(a-j) shows typical fracture surfaces of A380 deposits after heat treatment at different conditions at magnification of 2000× and 8000×. Figure 9(a) and (b) show the fracture surface morphologies of the as-sprayed A380 deposits. Some narrow apertures along particle boundaries can be observed, which would cause poor cohesion of particles. Decohesive rupture occurred, since the cracks mainly initiate at the interfaces of particles and no dimple rupture was observed. The particle bonding mechanism is mainly mechanical interlocking.

Figure 9(c) and (d) show that the fracture surfaces of samples heat treated at 200 °C display dimpled surfaces. This means the deposits began to become ductile and also confirms the stress–strain curves in Fig. 8. Furthermore, diffusion between particles takes place, and some strongly connected interfaces disappeared. The particle bonding mechanism begins to change to metallurgical bonding. This change can significantly improve the strength of interfaces, so the UTS of the deposits after heat treatment at 200 °C was much higher than that of as-sprayed deposits. However, some apertures and particles with incomplete deformation could still be observed, making the deposits fail at the early stage of tensile tests. This rupture can still be considered as decohesive rupture, since the cracks still occurred along the particle interfaces, although some dimples appeared as well.

Figure 9(e) and (f) show the fracture surfaces of deposits after heat treatment at 300 °C. Due to the removal of the work hardening along with recrystallization, as mentioned in "Microhardness" section, many deeper and larger dimples can be observed. This means that the degree

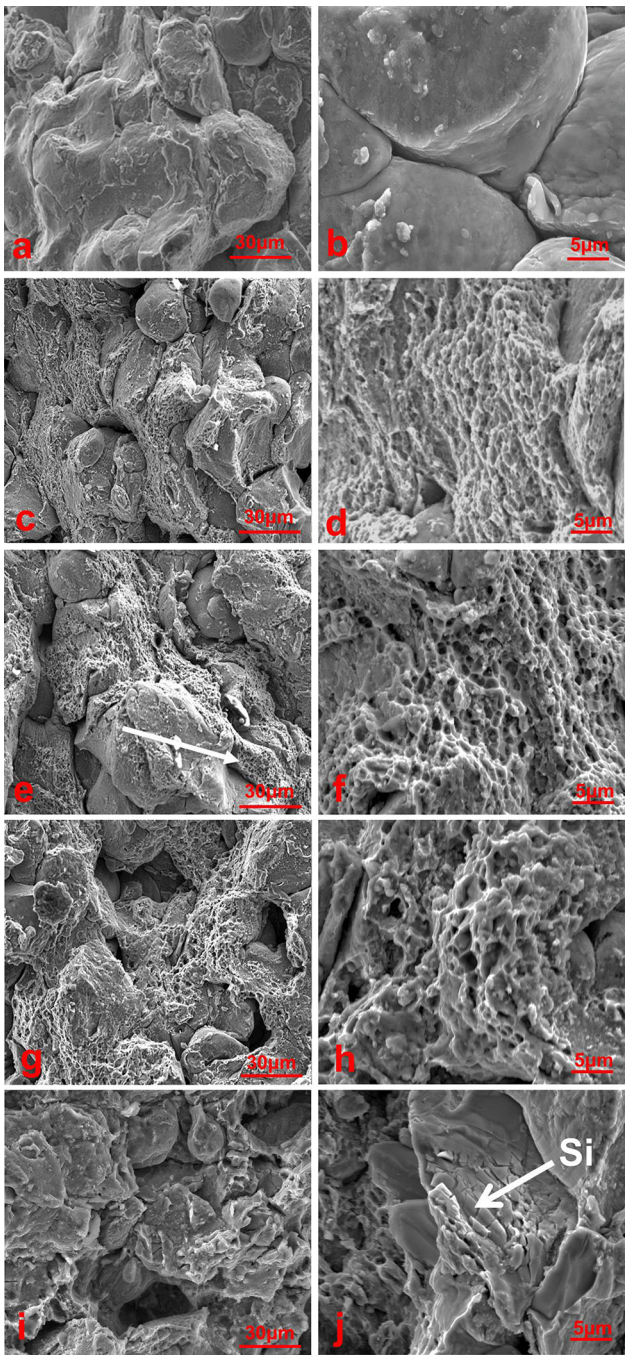

Fig. 9 Fracture surfaces (two magnifications) of tensile specimens of A380 deposits under as-deposited and heat treatment conditions

of intermetallic metallurgical bonding is increased. In Fig. 9(e), the deposit looks denser and the narrow apertures are converged to form a large pore. Moreover, some fractures occurred in the interior of the particles, as indicated by the white arrow, indicating that diffusion between particles was more complete and the deposit probably showed better ductility. However, weakly bonded interfaces still exist, which would significantly influence the diffusion as well as the strength of the deposit. Additionally, the high porosity may also lead to the rupture at an early stage during the tensile tests. Therefore, the strength and ductility of the deposits heat-treated at the 300 °C condition only increased slightly, as shown in Fig. 8. Huang et al. (Ref 15) called this kind of rupture "microvoid coalescence rupture" in their research.

In Fig. 9(g) and (h), obvious grain growth takes place for the 400 °C heat treatment condition, and the dimples get significantly larger. Literature (Ref 15) suggests that materials can plastically deform easily at lower strength after grain growth, and this is consistent with the stress–strain curves of the deposit heat treated at 400 °C, as shown in Fig. 8. The degree of diffusion between particles as well as the interior of particles further increases and compensates for the decrease of tensile properties caused by grain growth to a certain extent. Meanwhile, the pore sizes are further increased due to the convergence of apertures between particles. This indicated that it is difficult to eliminate the pores in cold-sprayed deposits simply by heat treatment.

Figure 9(i) and (j) show the significantly changed surface morphologies for the 500 °C heat treatment condition. The pores with large size still exist, while dimples can be observed only at higher magnification. The surface of the particles seems to be melted, which makes them look like de-shaped particles. The fracture surfaces of deposits exhibit mixed feature of cleavage and dimples. In Fig. 9(i), a lot of transgranular cracks can be observed. EDS measurements at high magnification indicated that cracks occurred at locations of Si aggregation. This is consistent with the optical micrograph of the deposits, in which Si grains gathered at particle boundaries for the 500 °C heat treatment condition. This kind of rupture is a mixture of microvoid coalescence–cleavage rupture. The cleavage fractures greatly reduce the plasticity of the material, which is consistent with the stress–strain curves shown in Fig. 8.

Conclusions

Cold spray was used to deposit A380 alloy powder onto a cylindrical steel substrate. The effects of heat treatment on the microstructure and mechanical properties of the deposits were investigated. The conclusions of this research can be summarized as follows:

1. With increase of the heat treatment temperature, the degree of diffusion of the elements increased and Si phase with mesh distribution experienced three stages: fragmentation, granulation, and coarsening, at 300, 400, and 500 °C, respectively. Besides, tiny pores at

particle boundaries converged and grew to size of 10 microns.
2. The microhardness showed a decreasing trend with increase of the heat treatment temperature, mainly due to elimination of work hardening and growth of Si phase.
3. Heat-treated samples showed better strength and ductility compared with the as-sprayed state. It was observed that the degree of intermetallic metallurgical bonding increased when removing work hardening along with recrystallization after heat treatment at suitable conditions. Material with optimum strength (186 ± 17 MPa) and elongation (0.93 ± 0.05 % Elf) was obtained by heat treatment at 300 and 400 °C, respectively.

Acknowledgment Financial support from the National Natural Science Foundation of China (No. 51671205) is gratefully acknowledged.

References

1. A. Papyrin, Cold Spray Technology, *Adv. Mater. Process.*, 2001, **159**, p 49-51
2. H. Assadi, F. Gartner, T. Stoltenhoff, and H. Kreye, Bonding Mechanism in Cold Gas Spraying, *Acta Mater.*, 2003, **51**, p 4379-4394
3. T. Stoltenhoff, H. Kreye, and H.J. Richter, An Analysis of the Cold Spray Process and Its Coatings, *J. Therm. Spray Technol.*, 2002, **11**, p 542-550
4. R.C. Dykhuizen, M.F. Smith, D.L. Gilmore, R.A. Neiser, X. Jiang, and S. Sampath, Impact of High Velocity Cold Spray Particles, *J. Therm. Spray Technol.*, 1999, **8**, p 559-564
5. Y. Hao, J.Q. Wang, X.Y. Cui, J. Wu, T.F. Li, and T.Y. Xiong, Microstructure Characteristics and Mechanical Properties of Al-12Si Coatings on AZ31 Magnesium Alloy Produced by Cold Spray Technique, *J. Therm. Spray Technol.*, 2016, **25**, p 1020-1028
6. M.R. Rokni, C.A. Widener, O.C. Ozdemir, and G.A. Crawford, Microstructure and Mechanical Properties of Cold Sprayed 6061 Al in As-Sprayed and Heat Treated Condition, *Surf. Coat. Technol.*, 2017, **309**, p 641-650
7. M.R. Rokni, C.A. Widener, V.K. Champagne, G.A. Crawford, and S.R. Nutt, The Effects of Heat Treatment on 7075 Al Cold Spray Deposits, *Surf. Coat. Technol.*, 2017, **310**, p 278-285
8. T. Suhonen, T. Varis, S. Dosta, M. Torrell, and J.M. Guilemany, Residual Stress Development in Cold Sprayed Al, Cu and Ti Coatings, *Acta Mater.*, 2013, **61**, p 6329-6337
9. S.R. Bakshi, D. Wang, T. Price, D. Zhang, A.K. Keshri, Y. Chen, D.G. McCartney, P.H. Shipway, and A. Agarwal, Microstructure and Wear Properties of Aluminum/Aluminum-Silicon Composite Coatings Prepared by Cold Spraying, *Surf. Coat. Technol.*, 2009, **204**, p 503-510
10. D. Poirier, J.G. Legoux, R.A.L. Drew, and R. Gauvin, Consolidation of Al_2O_3/Al Nanocomposite Powder by Cold Spray, *J. Therm. Spray Technol.*, 2011, **20**, p 275-284
11. A. List, F. Gartner, T. Mori, M. Schulze, H. Assadi, S. Kuroda, and T. Klassen, Cold Spraying of Amorphous Cu50Zr50 Alloys, *J. Therm. Spray Technol.*, 2015, **24**, p 108-118
12. A. Sova, S. Grigoriev, A. Okunkova, and I. Smurov, Potential of Cold Gas Dynamic Spray as Additive Manufacturing Technology, *Int. J. Adv. Manuf. Technol.*, 2013, **69**, p 2269-2278
13. Y. Cormier, P. Dupuis, A. Farjam, A. Corbeil, and B. Jodoin, Additive Manufacturing of Pyramidal Pin Fins: Height and Fin Density Effects Under Forced Convection, *Int. J. Heat Mass Transf.*, 2014, **75**, p 235-244
14. J.-H. Cho, Y.-M. Jin, D.-Y. Park, H.-J. Kim, I.-H. Oh, and K.-A. Lee, Manufacture and Properties of Cold Spray Deposited Large Thickness Cu Coating Material for Sputtering Target, *Met. Mater. Int.*, 2011, **17**, p 157-166
15. R.Z. Huang, M. Sone, W.H. Ma, and H. Fukanuma, The Effects of Heat Treatment on the Mechanical Properties of Cold-Sprayed Coatings, *Surf. Coat. Technol.*, 2015, **261**, p 278-288
16. P.D. Eason, J.A. Fewkes, S.C. Kennett, T.J. Eden, K. Tello, M.J. Kaufman, and M. Tiryakioglu, On the Characterization of Bulk Copper Produced by Cold Gas Dynamic Spray Processing in As-Fabricated and Annealed Conditions, *Mater. Sci. Eng. A*, 2011, **528**, p 8174-8178
17. Y. Yang, K.L. Yu, Y.G. Li, D.G. Zhao, and X.F. Liu, Evolution of Nickel-Rich Phases in Al-Si-Cu-Ni-Mg Piston Alloys with Different Cu Additions, *Mater. Des.*, 2012, **33**, p 220-225
18. C.-W. Yang, Y.-H. Chang, T.-S. Lui, and L.-H. Chen, Effects of Friction Stir Processing and Artificial Peak Aging on Erosion Resistance of Al-11Si-4Cu-2Ni-0.7Mg Cast Alloy, *Mater. Des.*, 2012, **40**, p 163-170
19. S. Tutunchilar, M. Haghpanahi, M.K. Besharati Givi, P. Asadi, and P. Bahemmat, Simulation of Material Flow in Friction Stir Processing of a Cast Al-Si Alloy, *Mater. Des.*, 2012, **40**, p 415-426
20. S. Tutunchilar, M.K. Besharati Givi, M. Haghpanahi, and P. Asadi, Eutectic Al-Si Piston Alloy Surface Transformed to Modified Hypereutectic Alloy Via FSP, *Mater. Sci. Eng. A*, 2012, **534**, p 557-567
21. J.Y. Hwang, H.W. Doty, and M.J. Kaufman, The Effects of Mn Additions on the Microstructure and Mechanical Properties of Al-Si-Cu Casting Alloys, *Mater. Sci. Eng. A*, 2008, **488**, p 496-504
22. X.X. Hou, H. Yang, Y. Zhao, and F.Z. Pan, Effect of Si on the Interaction Between Die Casting Die and Aluminum Alloy, *Mater. Lett.*, 2004, **58**, p 3424-3427
23. H.M. Guo, X.J. Yang, B. Hu, and G.L. Zhu, Rheo-Diecasting Process for Semi-Solid Aluminium Alloys, *J. Wuhan Univ. Technol.*, 2007, **22**, p 590-595
24. N. Saklakoglu, S. Gencalp, and S. Kasman, The Effects of Cooling Slope Casting and Isothermal Treatment on Wear Behavior of A380 Alloy, *Adv. Mater. Res.*, 2011, **264–265**, p 42-47
25. N. Saklakoglu, S. Gencalp, S. Kasman, and I.E. Saklakoglu, Formation of Globular Microstructure in A380 Aluminum Alloy by Cooling Slope Casting, *Adv. Mater. Res.*, 2011, **264–265**, p 272-277
26. F.H. Samuel, G. Pucella, C. Villeneuve, A.M. Samuel, H.W. Doty, and S. Valtierra, Microstructural Observations on Fe-Intermetallics in Unmodified and Sr-Modified Al-Si-Cu (A3801) Die Casting Alloy, *Int. J. Cast Met. Res.*, 1999, **12**, p 197-210
27. A. Wiengmoon, P. Sukchot, N. Tareelap, J.T.H. Pearce, and T. Chairuangsri, Effects of T6 Heat Treatment with Double Solution Treatment on Microstructure, Hardness and Corrosion Resistance of Cast Al-Si-Cu Alloy, *Arch. Metall. Mater.*, 2015, **60**, p 881-886
28. M. Karamouz, M. Azarbarmas, M. Emamy, and M. Alipour, Microstructure, Hardness and Tensile Properties of A380 Aluminum Alloy with and without Li Additions, *Mater. Sci. Eng. A*, 2013, **582**, p 409-414

29. H.L. Yang, S.X. Ji, and Z.Y. Fan, Effect of Heat Treatment and Fe Content on the Microstructure and Mechanical Properties of Die-Cast Al-Si-Cu Alloys, *Mater. Des.*, 2015, **85**, p 823-832
30. M. Rosso, I. Peter, C. Bivol, R. Molina, and G. Tonno, Development of Industrial Components by Advanced Squeeze Casting, *Int. J. Mater. Form.*, 2010, **3**, p 787-790
31. P. Coddet, C. Verdy, C. Coddet, F. Debray, and F. Lecouturier, Mechanical Properties of Thick 304L Stainless Steel Deposits Processed by He Cold Spray, *Surf. Coat. Technol.*, 2015, **277**, p 74-80
32. A.L.M. Bandar, P. Vo, R. Mongrain, E. Irissou, and S. Yue, Effect of Heat Treatment on the Microstructure and Mechanical Properties of Stainless Steel 316L Coatings Produced by Cold Spray for Biomedical Applications, *J. Therm. Spray Technol.*, 2014, **23**, p 641-652